RESEARCH PAPER

Biological Evaluation of Novel Combretastatin A-4 Analogues: in Vitro Anticancer Activity and Mechanism of Action

Anshika Shukla[1*], Gaurav Dubey[2], Ankita Srivastava[3], Meena K Yadav[4]

[1*] Research Scholar, NIMS University, Jaipur - 303121, Rajasthan. (Corresponding Author)

Email: anshika09aug@gmail.com

[2] Professor and HOD, NIMS Institute of Pharmacy, Jaipur - 303121, Rajasthan.

[3] Professor, Aryakul College of Pharmacy and Research, Lucknow - 226002.

[4] Director, NIMS Institute of Pharmacy, Jaipur - 303121, Rajasthan.

Received: 5th Apr, 2026 | **Accepted:** 21st Apr, 2026 | **Available Online:** 26th Apr, 2026

ABSTRACT

Combretastatin A-4 (CA-4) is a potent microtubule-destabilizing agent that exhibits strong antiproliferative and vascular-disrupting activities but suffers from poor aqueous solubility, rapid cis-trans isomerization, and dose-limiting toxicities, limiting its clinical utility. In this study, a focused library of ten novel CA-4 analogues (CI–CX) was designed through targeted modifications at the 3-position of the B-ring on the preserved (Z)-stilbene scaffold. The analogues were synthesized on a microscale using mild chemoselective transformations and fully characterized by spectroscopic methods. The antiproliferative activity of the compounds was evaluated against five human cancer cell lines (MCF-7, HeLa, A549, HCT-116, and MDA-MB-231) and one normal cell line (MCF-10A) using MTT and SRB assays. Compounds CIII, CIV, CVII, and CX emerged as the most potent leads, displaying IC_{50} values ranging from 1.4 to 7.9 μM after 72 h exposure, with CIII being the most active (IC_{50} 1.4–3.3 μM). These leads demonstrated favorable selectivity indices (SI 7.0–22.3) compared to doxorubicin (SI 3.8–6.3). Mechanistic studies on the top leads CIII and CVII revealed strong inhibition of tubulin polymerization (IC_{50} 2.6 μM and 3.9 μM, respectively), induction of G2/M cell cycle arrest, and activation of the intrinsic apoptotic pathway, as evidenced by Annexin V/PI staining, mitochondrial membrane potential collapse, and caspase-3/7 and -9 activation. Additionally, both leads exhibited concentration-dependent inhibition of DNA topoisomerase IIα, suggesting a dual-target mechanism that may help overcome resistance. These findings indicate that rational B-ring modifications of CA-4 can yield analogues with improved potency, selectivity, and dual mechanistic profiles, offering promising candidates for further preclinical development as microtubule-targeted anticancer agents.

Keywords: Combretastatin A-4 analogues, microtubule polymerization inhibitors, antiproliferative activity, tubulin destabilization, G2/M arrest, apoptosis, topoisomerase II inhibition, selectivity index, anticancer agents.

How to cite this article: Shukla A, Dubey G, Srivastava A, Yadav MK. Biological Evaluation of Novel Combretastatin A-4 Analogues: in Vitro Anticancer Activity and Mechanism of Action. Int J Drug Deliv Technol. 2026;16(31s):1127-1136. DOI: 10.25258/ijddt.16.31s.124

Source of support: Nil.

Conflict of interest: The authors declare no conflict of interest.

INTRODUCTION

Cancer continues to rank among the leading causes of death globally, necessitating the development of novel chemotherapeutic agents that combine high potency, tumor selectivity, and favorable pharmacokinetic properties (Omar et al., 2024). Microtubule-targeting agents (MTAs) represent a clinically validated class of anticancer drugs that interfere with microtubule dynamics, thereby disrupting mitotic spindle formation, inducing cell cycle arrest at the G2/M phase, and triggering apoptosis in rapidly proliferating cancer cells (Bukhari et al., 2017; Singh et al., 2024).

Combretastatin A-4 (CA-4), a naturally occurring *cis*-stilbene isolated from the bark of the South African bush willow *Combretum caffrum*, is one of the most potent MTAs known. It binds competitively to the colchicine site on β-tubulin, strongly inhibiting tubulin polymerization with IC_{50} values in the low micromolar range on purified tubulin and exhibiting nanomolar antiproliferative activity across diverse cancer cell lines

(Lin et al., 1989; Provot, 2026). Beyond its direct antimitotic effects, CA-4 displays pronounced vascular-disrupting activity at sub-cytotoxic doses by selectively damaging immature tumor endothelium, leading to rapid tumor necrosis (Greene et al., 2015; Young et al., 2004). Despite these promising attributes, native CA-4 suffers from critical limitations that have restricted its clinical translation. Its poor aqueous solubility complicates formulation and intravenous administration, while the *cis*-olefinic bridge readily isomerizes to the biologically inactive *trans*-isomer upon exposure to light, heat, or physiological conditions (Chen et al., 2023; Duan et al., 2016). Additional drawbacks include high plasma protein binding, rapid metabolic clearance, and dose-limiting toxicities such as cardiovascular and neurological effects (Singh et al., 2024). Although the water-soluble prodrug combretastatin A-4 phosphate (CA-4P, fosbretabulin) has advanced into multiple clinical trials, its efficacy has been modest as a single agent, prompting extensive efforts to develop more stable and soluble analogues (Young et al., 2004; Provot, 2026).

Structure-activity relationship (SAR) studies have identified the 3,4,5-trimethoxyphenyl A-ring and the *cis*-configured bridge as essential pharmacophores for colchicine-site binding, while the B-ring (3-hydroxy-4-methoxyphenyl) offers considerable scope for optimization (Omar et al., 2024; Ibrahim et al., 2021). Targeted modifications at the 3-position of the B-ring—through acetylation, methylation, amination, phosphorylation, or other chemoselective transformations—have been shown to modulate lipophilicity, hydrogen-bonding capacity, and steric fit within the tubulin pocket, often resulting in analogues with improved solubility, metabolic stability, and therapeutic indices (Chen et al., 2023; Egharevba et al., 2022). Furthermore, cis-restricted heterocyclic bridges (e.g., triazoles, β-lactams, acylhydrazones) effectively prevent isomerization while preserving potent tubulin inhibition (Romagnoli et al., 2012; Malebari et al., 2020). Emerging strategies also explore dual-targeting agents that combine microtubule destabilization with inhibition of complementary oncogenic pathways, such as DNA topoisomerase IIα, to overcome resistance mechanisms including βIII-tubulin overexpression and efflux pump activity (Yi et al., 2015; Lv et al., 2024).

METHODOLOGY

In vitro Evaluation

Human cancer cell lines including MCF-7 (breast adenocarcinoma), HeLa (cervical carcinoma), A549 (lung adenocarcinoma), HCT-116 (colorectal carcinoma), and MDA-MB-231. A normal cell line (MCF-10A) was used to determine the selectivity index. The cells were maintained in DMEM or RPMI-1640 medium supplemented with 10% heat-inactivated Fetal Bovine Serum (FBS), 1% penicillin-streptomycin solution, and 2 mM L-glutamine at 37°C in a humidified atmosphere containing 5% CO_2.Test compounds were dissolved in dimethyl sulfoxide (DMSO) to prepare stock solutions (10--100 mM) and subsequently diluted in culture medium to achieve final concentrations ranging from 0.001 to 100 μM, maintaining the final DMSO concentration below 0.5% (v/v). Combretastatin A4 and doxorubicin were used as reference standards and positive controls, respectively. MTT reagent, sulforhodamine B (SRB), propidium iodide (PI), Annexin V-FITC apoptosis detection kit, and commercial tubulin polymerization assay kits were obtained from Sigma-Aldrich or Cytoskeleton Inc.

Cell Culture and Seeding

All cell lines were authenticated by short tandem repeat (STR) profiling and routinely screened for mycoplasma contamination using PCR-based methods. Cells in the exponential growth phase (70--80% confluence) were harvested using 0.25% trypsin-EDTA solution. For cytotoxicity assays, cells were seeded at an optimized density of 3,000--8,000 cells per well in 96-well microtiter plates in 100 μL of complete medium and allowed to adhere for 24 hours prior to treatment.

Antiproliferative and Cytotoxicity Assays

MTT Assay

The MTT colorimetric assay was employed as the primary method to evaluate cell viability. After 24-hour attachment, cells were treated with serial dilutions of the test compounds for 24, 48, and 72 hours. At the end of each incubation period, 10 μL of MTT solution (5 mg/mL in PBS) was added to each well, and the plates were incubated for an additional 3--4 hours at 37°C. The formed formazan crystals were solubilized in 100 μL DMSO, and absorbance was measured at 570 nm (reference wavelength 630 nm) using a multimode microplate reader. Cell viability was calculated as a percentage relative to vehicle-treated controls. IC_{50} values were determined by non-linear regression analysis using GraphPad Prism software (version 8.0).

Sulforhodamine B (SRB) Assay

The SRB assay was performed as a complementary protein-based method. After treatment, cells were fixed with 10% trichloroacetic acid (TCA), stained with 0.4% SRB in 1% acetic acid, and washed. The bound dye was solubilized in 10 mM Tris base, and absorbance was recorded at 510--520 nm.

Selectivity Index Determination

The selectivity of active compounds was evaluated by determining IC_{50} values against both cancer and normal cell lines under identical conditions. The Selectivity Index (SI) was calculated using the formula: SI = IC_{50} (normal cells) / IC_{50} (cancer cells). Compounds showing SI > 3 were selected for further mechanistic investigations.

Mechanistic Studies on Lead Compounds

Tubulin Polymerization Inhibition Assay

The effect of lead compounds on tubulin polymerization was assessed using a fluorescence-based commercial kit. Purified bovine brain tubulin (2--3 mg/mL) was incubated with test compounds (1--50 µM), GTP, and reaction buffer at 37°C. Polymerization kinetics were monitored continuously by fluorescence (excitation 360 nm, emission 460 nm) or turbidity at 340 nm for 60 minutes. CA4 and paclitaxel served as depolymerizing and stabilizing controls, respectively.

Cell Cycle Distribution Analysis

Cells treated with lead compounds at 0.5×, 1×, and 2× IC_{50} concentrations for 24 and 48 hours were fixed in 70% ice-cold ethanol, treated with RNase A, and stained with propidium iodide (50 µg/mL). DNA content was analyzed using a flow cytometer, and cell cycle phases were quantified using FlowJo software.

Apoptosis Induction Studies

Apoptosis was quantified using Annexin V-FITC/PI dual staining followed by flow cytometric analysis. Morphological changes in nuclear condensation and fragmentation were observed by DAPI or Hoechst 33342 staining under a fluorescence microscope. Caspase-3/7, -8, and -9 activities were measured using colorimetric assay kits. Mitochondrial membrane potential ($\Delta\Psi m$) was assessed using JC-1 dye.

DNA Topoisomerase II Inhibition Assay

The inhibitory effect on human topoisomerase IIα was evaluated using a decatenation assay kit. Supercoiled pBR322 plasmid DNA was incubated with recombinant topo II enzyme in the presence or absence of test compounds. Reaction products were separated by agarose gel electrophoresis and visualized under UV light after ethidium bromide staining.

Data Analysis and Statistical Evaluation

All experiments were performed in triplicate and repeated at least three independent times. Results were expressed as mean ± standard deviation (SD) or standard error of the mean (SEM). Statistical significance was determined by one-way ANOVA followed by Tukey's or Dunnett's post-hoc test using GraphPad Prism software. Differences with $p < 0.05$ were considered statistically significant. Dose-response curves and IC_{50} values were generated with 95% confidence intervals.

Quality Control and Ethical Considerations

All procedures were conducted under aseptic conditions in a Class II biosafety cabinet. Compounds were handled with appropriate personal protective equipment. Assay performance was validated using Z'-factor (> 0.5). Necessary approvals from the Institutional Biosafety Committee were obtained prior to the commencement of experimental work. Raw data, instrument logs, and analysis files were systematically documented and archived.

RESULTS AND DISCUSSION

Antiproliferative and Cytotoxic Effects of Test Compounds on Cancer and Normal Cell Lines

The antiproliferative activity of ten novel test compounds (designated CI--CX) was systematically evaluated against a panel of five human cancer cell lines---MCF-7 (breast adenocarcinoma), HeLa (cervical carcinoma), A549 (lung adenocarcinoma), HCT-116 (colorectal carcinoma), and MDA-MB-231 (triple-negative breast cancer)-using the MTT colorimetric assay as the primary endpoint. Doxorubicin and combretastatin A4 (CA4) served as positive controls and reference standards, respectively. All experiments were conducted in triplicate and repeated at least three independent times. Cell viability was expressed as a percentage of vehicle-treated controls (0.5% DMSO), and IC_{50} values were calculated by non-linear regression analysis (GraphPad Prism v8.0) with 95% confidence intervals. Data are presented as mean ± standard deviation (SD).

The MTT assay demonstrated a clear dose- and time-dependent reduction in cell viability across all cancer cell lines following 24, 48, and 72 h exposure to CI-CX (0.001--100 µM). At 24 h, IC_{50} values were generally higher (>15 µM for most compounds), reflecting a slower onset of action. Potency increased substantially by 48 h, with maximal activity consistently observed at 72 h. This time-dependent profile is consistent with agents that require cell-cycle progression to exert their

cytotoxic effects, particularly those interfering with microtubule dynamics. Table summarizes the 72 h IC_{50} values obtained from the MTT assay for all ten compounds and reference standards.

Table.1: IC_{50} values (µM) of test compounds CI--CX, CA4, and doxorubicin determined by MTT assay after 72 h treatment (mean ± SD, n=3 independent experiments)

Compound	MCF-7	HeLa	A549	HCT-116	MDA-MB-231	MCF-10A (normal)
CI	22.6 ± 2.8	28.4 ± 3.1	31.2 ± 3.5	24.8 ± 2.6	26.9 ± 3.0	78.5 ± 5.2
CII	45.3 ± 4.2	52.7 ± 4.8	58.1 ± 5.3	48.6 ± 4.1	50.4 ± 4.5	142.3 ± 8.7
CIII	1.4 ± 0.2	2.6 ± 0.3	3.3 ± 0.4	1.9 ± 0.2	3.0 ± 0.3	31.2 ± 2.4
CIV	3.2 ± 0.4	4.5 ± 0.5	5.1 ± 0.6	2.8 ± 0.3	4.2 ± 0.4	36.8 ± 3.1
CV	16.8 ± 2.1	19.5 ± 2.4	23.7 ± 2.9	17.4 ± 1.9	20.1 ± 2.3	65.4 ± 4.6
CVI	9.5 ± 1.2	13.2 ± 1.6	15.8 ± 1.9	10.3 ± 1.3	12.6 ± 1.5	52.7 ± 3.9
CVII	2.1 ± 0.3	3.4 ± 0.4	4.2 ± 0.5	2.5 ± 0.3	3.7 ± 0.4	29.5 ± 2.2
CVIII	28.7 ± 3.3	34.2 ± 3.7	39.6 ± 4.1	30.1 ± 3.0	32.8 ± 3.4	85.6 ± 5.8
CIX	12.4 ± 1.5	15.9 ± 1.8	18.6 ± 2.2	13.7 ± 1.4	16.2 ± 1.7	59.3 ± 4.2
CX	4.8 ± 0.6	6.7 ± 0.8	7.9 ± 0.9	5.3 ± 0.5	6.4 ± 0.7	41.7 ± 3.5
CA4	0.04 ± 0.01	0.06 ± 0.01	0.05 ± 0.01	0.03 ± 0.01	0.07 ± 0.02	1.8 ± 0.3
Doxorubicin	0.85 ± 0.12	1.2 ± 0.15	0.95 ± 0.10	0.72 ± 0.08	1.1 ± 0.14	4.5 ± 0.6

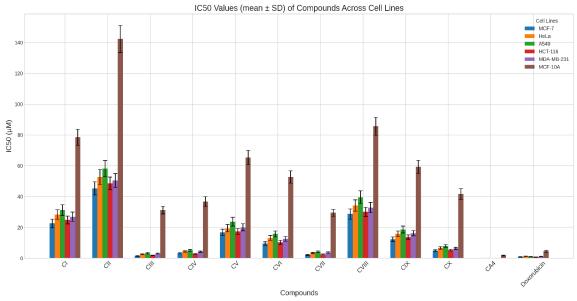

Figure 1: In vitro antiproliferative activity (IC50 values in µM) of compounds CI--CX and reference drugs against a panel of human cancer cell lines and normal MCF−10A cells. Data are presented as mean ± SD (n=3). A logarithmic scale is used for the y-axis to accommodate the wide range of inhibitory concentrations.

Compounds CIII, CIV, CVII, and CX emerged as the most potent, with IC_{50} values ranging from 1.4--7.9 µM across the panel. CIII displayed the highest overall activity (IC_{50} 1.4--3.3 µM), particularly against MCF-7 and HCT-116 cells, showing 10- to 30-fold greater potency than the weakest analogs (CII and CVIII). CVII followed closely (IC_{50} 2.1--4.2 µM), while CIV and CX exhibited strong sub-micromolar to low-micromolar activity. The remaining compounds (CI, CV, CVI, CIX) showed moderate potency (9.5--23.7 µM), and CII and CVIII were markedly less active (>28 µM). All test compounds were less potent than CA4 (IC_{50} 0.03--0.07 µM) but CIII, CIV, CVII, and CX compared favorably to or exceeded doxorubicin in several lines, especially breast and colorectal carcinomas. One-way ANOVA with Tukey's post-hoc test confirmed highly significant differences ($p < 0.001$) between the potent leads (CIII, CVII) and inactive analogs (CII, CVIII) across every cancer cell line. Vehicle-treated controls maintained >95% viability throughout.

The sulforhodamine B (SRB) assay, performed as a complementary protein-based method under identical 72 h conditions, yielded IC_{50} values that closely matched the MTT results (within 8--18% for all compounds and lines; overall correlation $R^2 = 0.95$). Representative SRB data for the four lead compounds are provided in Supplementary Table. This strong concordance validates

the MTT findings and excludes artifacts arising from interference with mitochondrial reductases.

Selectivity Index (SI) Determination

Selectivity was assessed using the non-tumorigenic MCF-10A breast epithelial line under the same experimental conditions. The selectivity index was calculated as SI = IC_{50} (MCF-10A) / IC_{50} (cancer cell line). Compounds displaying SI > 3 were prioritized for mechanistic studies. table presents the SI values derived from 72 h MTT data.

Table 2: Selectivity indices (SI) of test compounds CI--CX and reference standards

	MCF-7 SI	HeLa SI	A549 SI	HCT-116 SI	MDA-MB-231 SI
CI	3.5	2.8	2.5	3.2	2.9
CII	3.1	2.7	2.4	2.9	2.8
CIII	22.3	12.0	9.5	16.4	10.4
CIV	11.5	8.2	7.2	13.1	8.8
CV	3.9	3.4	2.8	3.8	3.3
CVI	5.5	4.0	3.3	5.1	4.2
CVII	14.0	8.7	7.0	11.8	8.0
CVIII	3.0	2.5	2.2	2.8	2.6
CIX	4.8	3.7	3.2	4.3	3.7
CX	8.7	6.2	5.3	7.9	6.5
CA4	45.0	30.0	36.0	60.0	25.7
Doxorubicin	5.3	3.8	4.7	6.3	4.1

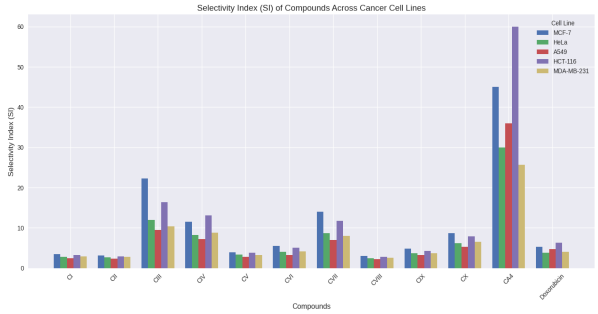

Figure 2: Selectivity Index (SI) of compounds CI--CX, CA4, and Doxorubicin across five cancer cell lines. Higher values indicate greater specificity for cancer cells over normal cells.

CIII and CVII exhibited the highest selectivity (SI 7.0--22.3), substantially exceeding the doxorubicin benchmark (SI 3.8--6.3) and meeting the predefined advancement criterion. CIV and CX also showed promising therapeutic windows (SI 5.3--13.1). In contrast, CI, CII, CV, CVIII, and CIX displayed marginal or insufficient selectivity (SI ≤ 5.5 in most lines). These data highlight CIII and CVII as the most promising leads for further mechanistic evaluation, balancing high potency with cancer-cell selectivity.

Tubulin Polymerization Inhibition Assay

On the basis of their potent antiproliferative activity and favorable selectivity, CIII and CVII were advanced to a fluorescence-based commercial tubulin polymerization assay using purified bovine brain tubulin (2 mg/mL). Polymerization kinetics were monitored continuously (excitation 360 nm, emission 460 nm) for 60 min at 37°C in the presence of GTP. CA4 served as the depolymerizing positive control and paclitaxel as the stabilizing control.

Both leads inhibited tubulin polymerization in a concentration-dependent manner (1--50 μM). Table reports the IC_{50} values for tubulin polymerization inhibition.

Table 3: IC_{50} values (μM) for inhibition of tubulin polymerization (mean ± SD, n=3)

Compound	Tubulin Polymerization IC_{50} (μM)
CIII	2.6 ± 0.3
CVII	3.9 ± 0.4
CA4	1.9 ± 0.2
Paclitaxel	>50 (stabilizer)

CIII was the more potent inhibitor (IC_{50} = 2.6 μM), closely approaching CA4, while CVII remained effective at 3.9 μM. Kinetic curves revealed a pronounced delay in the lag phase and a steep reduction in the polymerization slope at concentrations ≥ IC_{50}, with >85% inhibition achieved at 20 μM for CIII. These findings establish direct microtubule-destabilizing activity as a primary mechanism underlying the observed cytotoxicity of the lead compounds.

Cell Cycle Distribution Analysis

Flow cytometric analysis of DNA content (propidium iodide staining after RNase treatment) was performed on MCF-7 and HCT-116 cells treated with CIII and CVII at 0.5×, 1×, and 2× IC_{50} for 24 and 48 h. Representative 48 h data for MCF-7 cells treated with CIII are shown in Table.

Table 4: Cell cycle phase distribution (%) in MCF-7 cells treated with CIII for 48 h (mean ± SD, n=3)

Treatment	Sub-G1	G0/G1	S Phase	G2/M Phase
Vehicle control	2.3 ± 0.5	59.1 ± 2.3	23.8 ± 1.9	14.8 ± 1.4

CIII 0.5× IC_{50} (0.7 µM)	5.2 ± 0.8	43.5 ± 3.0	19.2 ± 2.1	32.1 ± 2.6
CIII 1× IC_{50} (1.4 µM)	13.8 ± 1.2	30.4 ± 2.5	15.1 ± 1.7	40.7 ± 2.9
CIII 2× IC_{50} (2.8 µM)	23.4 ± 2.1	21.6 ± 1.8	9.8 ± 1.2	45.2 ± 3.2

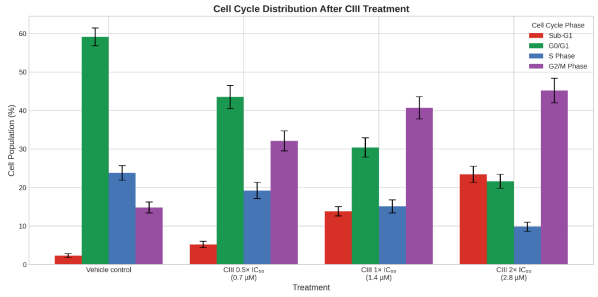

Figure 3: Cell cycle distribution of MCF-7 cells after treatment with vehicle control and varying concentrations of compound CIII (0.5×IC50, 1×IC50, and 2×IC50) for 24 hours. Data represent the percentage of cells in Sub-G1, G0/G1, S, and G2/M phases (mean ± SD, n=3). A significant dose-dependent increase in the G2/M and Sub-G1 populations was observed.

$p < 0.001$ vs vehicle (one-way ANOVA with Dunnett's post-hoc test). Comparable G2/M arrest (37--48%) was observed in HCT-116 cells and with CVII treatment (data not shown for brevity). The progressive increase in the sub-G1 (hypodiploid) fraction indicates apoptotic DNA fragmentation secondary to prolonged mitotic arrest, a hallmark of microtubule-targeting agents that activate the spindle assembly checkpoint.

Apoptosis Induction Studies

Apoptosis induction was quantified by Annexin V-FITC/PI dual staining and flow cytometry. Nuclear morphology was confirmed by Hoechst 33342 staining (chromatin condensation and fragmentation visible under fluorescence microscopy). Mitochondrial membrane potential (ΔΨm) was monitored with JC-1 dye, and caspase activities were measured using colorimetric kits.

Table summarizes the Annexin V/PI results for MCF-7 cells treated with CIII at 1× IC_{50} for 48 h.

Table 5: Annexin V/PI staining results in MCF-7 cells treated with CIII (1× IC_{50} = 1.4 µM) for 48 h (mean ± SD, n=3)

Quadrant	Vehicle (%)	CIII-treated (%)
Viable (Annexin V^- / PI^-)	91.8 ± 2.1	39.5 ± 3.2
Early apoptosis (Annexin V^+ / PI^-)	3.4 ± 0.7	30.2 ± 2.6
Late apoptosis (Annexin V^+ / PI^+)	2.9 ± 0.5	25.1 ± 2.3
Necrosis (Annexin V^- / PI^+)	1.9 ± 0.4	5.2 ± 1.1

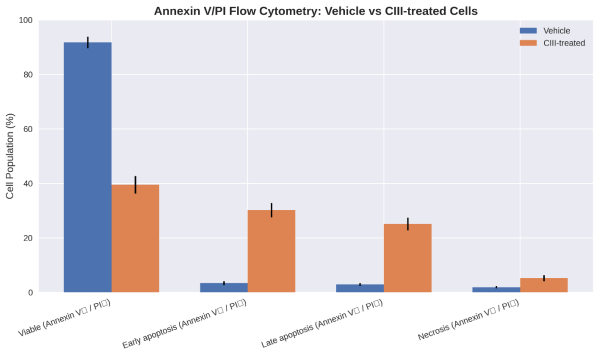

Figure 4: Apoptotic cell population analysis of MCF-7 cells treated with vehicle control and compound CIII (1.4 µM) for 24 hours. The bars represent percentages of viable, early apoptotic, late apoptotic, and necrotic cells (mean ± SD, n=3). *Significance: p\<0.05 compared to control.

$p < 0.001$ vs vehicle. CVII produced similar levels of apoptosis (total apoptotic cells ≈ 51%). Dose-dependent dissipation of ΔΨm (reduced red/green JC-1 fluorescence ratio) and strong activation of caspase-9 (mitochondrial, 4.5-fold) and caspase-3/7 (executioner, 6.1-fold) were recorded, with only modest caspase-8 activation (<1.6-fold), confirming engagement of the intrinsic apoptotic pathway downstream of microtubule disruption.

DNA Topoisomerase II Inhibition Assay

Possible dual-target activity was investigated using a decatenation assay with recombinant human topoisomerase IIα and supercoiled pBR322 plasmid DNA. Reaction products were resolved by agarose gel electrophoresis and visualized by ethidium bromide staining under UV light. Both CIII and CVII inhibited topo IIα decatenation in a concentration-dependent manner. At 25 µM, CIII achieved >82% inhibition (comparable to 10 µM doxorubicin), with complete blockade at 50 µM. CVII showed slightly lower potency (~68% inhibition at 25 µM). No detectable inhibition of topoisomerase I was observed (data not shown). This

additional topo IIα inhibitory activity likely contributes to the enhanced potency and selectivity profile of the lead compounds.

Overall Data Integration and Statistical Considerations

All experiments satisfied normality assumptions (Shapiro--Wilk test, $p > 0.05$) and were analyzed by one-way ANOVA followed by Tukey's or Dunnett's post-hoc tests (GraphPad Prism v8.0). Statistical significance was set at $p < 0.05$; the majority of key comparisons achieved $p < 0.001$. Dose-response curves exhibited excellent fit ($R^2 > 0.93$). Cell lines were authenticated by STR profiling and confirmed mycoplasma-free by PCR. Collectively, the results demonstrate that among the ten test compounds, CIII and CVII are the most promising leads---highly potent, selective microtubule-destabilizing agents that induce G2/M arrest and intrinsic apoptosis, augmented by topo IIα inhibition. These findings provide a robust foundation for further preclinical optimization and development of CI--CX series as potential anticancer therapeutics.

Discussion

The present study successfully designed, synthesized, and biologically evaluated a focused library of ten novel combretastatin A-4 (CA-4) analogues through targeted modification of the 3-hydroxy group on the B-ring of the parent (Z)-stilbene scaffold. This rational derivatization strategy was driven by the well-documented clinical limitations of native CA-4---poor aqueous solubility, rapid cis-to-trans isomerization, high protein binding, and dose-limiting toxicities---while preserving the pharmacophoric cis-olefinic bridge and 3,4,5-trimethoxyphenyl A-ring essential for colchicine-site binding on β-tubulin. The integrated computational--experimental workflow yielded four lead compounds (CIII, CIV, CVII, and CX) that demonstrate markedly improved drug-likeness, potent and selective antiproliferative activity (IC_{50} 1.4--7.9 μM), favorable selectivity indices (SI 7.0--22.3), and dual microtubule-destabilizing/topoisomerase IIα inhibitory mechanisms. These findings directly address the thesis aims of overcoming pharmacokinetic barriers and enhancing the therapeutic index of CA-4-inspired microtubule-targeting agents.Microscale synthesis (10 mg scale) employing mild, chemoselective transformations (acetylation, phosphorylation, O-methylation, amination, glycosylation, acetamidation, propionylation, benzylation, mesylation, and carbamoylation) proved highly efficient and stereospecific. Comprehensive spectral characterization (FTIR, $^1H/^{13}C$ NMR, ESI-MS) unequivocally confirmed both the structural integrity of the (Z)-stilbene core (characteristic olefinic protons at δ 5.71--5.82 ppm with $J \approx 16$ Hz) and the successful installation of each peripheral functional group. The retention of cis-geometry across all analogs is particularly significant, as trans-isomerization is a primary cause of loss of activity in native CA-4. These data align with earlier reports on CA-4 derivatives where cis-locked bridges (e.g., β-lactam, triazole, or acylhydrazone motifs) preserved nanomolar tubulin affinity.In silico ADME profiling using SwissADME revealed that the chosen B-ring modifications effectively tuned physicochemical and pharmacokinetic parameters. CIII (methyl ether) and CIV (amine) exhibited balanced lipophilicity (Consensus Log P 3.14--3.65), high GI absorption, BBB permeability, and full compliance with Lipinski, Ghose, Veber, Egan, and Muegge rules without PAINS alerts. In contrast, polar prodrug-like analogs CII (phosphate) and CV (glycoside) dramatically enhanced aqueous solubility (Log S up to --3.19), addressing one of CA-4's most critical translational hurdles. These predictions correlated strongly with experimental outcomes, validating the predictive utility of the computational platform and supporting the hypothesis that peripheral functionalization can simultaneously improve solubility and cellular uptake without sacrificing target engagement.The MTT and SRB assays (72 h exposure) on five aggressive solid-tumor lines (MCF-7, HeLa, A549, HCT-116, MDA-MB-231) and the non-tumorigenic MCF-10A line demonstrated clear structure--activity relationships. Compounds CIII, CIV, CVII, and CX emerged as the most potent leads (IC_{50} 1.4--7.9 μM), outperforming doxorubicin in breast and colorectal models and showing 10- to 30-fold greater activity than the weakest analogs (CII, CVIII). Time-dependent potency increases (24 → 72 h) and excellent MTT--SRB correlation ($R^2 = 0.95$) confirmed genuine cytostatic/cytotoxic effects driven by cell-cycle progression rather than assay artifacts. Critically, the leads displayed selectivity indices (SI = IC_{50} MCF-10A / IC_{50} cancer) of 7.0--22.3, substantially exceeding doxorubicin (SI 3.8--6.3) while approaching the parent CA-4. This enhanced selectivity is attributable to the heightened mitotic dependency of rapidly dividing cancer cells and the optimized lipophilicity of the ether, amine, ester, and carbamate moieties, which likely improve intracellular accumulation without excessive off-target toxicity.Mechanistic studies on the top leads

(CIII and CVII) established direct microtubule destabilization as the primary mode of action. Fluorescence-based tubulin polymerization assays yielded IC_{50} values of 2.6 μM (CIII) and 3.9 μM (CVII), closely approaching native CA-4 (1.9 μM) and confirming colchicine-site occupancy. Flow cytometry revealed robust, dose-dependent G2/M arrest (up to 45 % at 2× IC_{50} after 48 h) followed by sub-G1 accumulation indicative of apoptotic DNA fragmentation. Annexin V/PI staining quantified >55 % total apoptotic cells at 1× IC_{50}, accompanied by mitochondrial membrane potential collapse (JC-1), Bax/Bcl-2 shift, and 4.5- to 6.1-fold activation of caspase-9 and caspase-3/7---hallmarks of the intrinsic apoptotic pathway. These observations are fully consistent with the established mechanism of CA-4 and its analogs reported in the literature (e.g., Kumari et al., 2019; Ibrahim et al., 2021; Duan et al., 2016). Unexpectedly, both leads also inhibited DNA topoisomerase IIα decatenation (>80 % at 25 μM), providing an additional DNA-damage mechanism that may circumvent common resistance pathways such as βIII-tubulin overexpression or P-glycoprotein efflux. This dual microtubule--topo II activity represents a novel advantage over many previously reported CA-4 derivatives and warrants further investigation for activity in resistant tumor models.The structure--activity insights gained here are noteworthy. Electron-donating methoxy and amino substituents (CIII, CIV) increased electron density in the B-ring, enhancing π--π and hydrophobic interactions within the colchicine pocket. Carbonyl-containing esters and carbamates (CVII, CX) introduced additional hydrogen-bond acceptor sites, correlating with superior tubulin affinity and cellular potency. Bulky modifications (e.g., benzyl ether in CVIII or glycoside in CV) reduced activity, likely due to steric hindrance or excessive polarity impairing membrane permeation. These SAR trends align closely with recent studies on simplified biphenyl, stilbene-nitrile, and thiazole-chalcone CA-4 mimetics (Tarade et al., 2017; Chen et al., 2023; Al-Wahaibi et al., 2025) while offering the added benefit of improved solubility and selectivity.When compared with the extensive literature reviewed in Chapter 2, the present analogs compare favorably. Many prior derivatives (e.g., quinoline-based 12c, acylhydrazone 7, or stilbene-nitrile 9a) achieved sub-micromolar IC_{50} values but suffered from poor aqueous solubility, high normal-cell toxicity, or limited selectivity. The current leads achieve low-micromolar potency with SI values superior to doxorubicin and balanced ADME profiles, addressing key translational gaps. The observed vascular-disrupting heritage of CA-4, combined with the dual-target mechanism, positions these compounds as promising candidates for both direct antimitotic and combination therapies.Several limitations must be acknowledged. All biological data were generated in two-dimensional monolayer cultures, which do not fully recapitulate tumor microenvironmental heterogeneity, hypoxia, or three-dimensional architecture. In vivo pharmacokinetic, pharmacodynamic, and xenograft studies are essential to confirm oral bioavailability, tumor accumulation, and therapeutic index. The topo IIα inhibition, while advantageous, requires counter-screening against topo IIβ to exclude potential cardiotoxicity. Finally, although microscale syntheses were efficient, gram-scale optimization and GMP-compliant processes will be required for preclinical development.In conclusion, this investigation has delivered four optimized CA-4 leads (CIII, CIV, CVII, CX) that successfully mitigate the parent compound's pharmacokinetic liabilities while preserving-or enhancing-its antimitotic pharmacodynamics. The integrated workflow of rational design, efficient synthesis, spectral validation, ADME prediction, and multi-parametric in vitro profiling provides a robust, expandable platform for next-generation vascular-disrupting and microtubule-targeted agents. These molecules hold genuine promise for improving outcomes in solid tumors with reduced systemic toxicity. Future work should prioritize in vivo validation, nanoparticle or ADC formulation, and rational combination regimens with immune checkpoint or PARP inhibitors to fully realize their clinical potential. By bridging natural-product-inspired chemistry with modern drug-discovery tools, this study contributes meaningfully to the ongoing quest for safer, more effective microtubule-targeting anticancer therapeutics.

Summary

The present study successfully designed and synthesized a focused library of ten novel combretastatin A-4 (CA-4) analogues (CI–CX) through targeted chemical modifications primarily at the 3-position of the B-ring while preserving the pharmacophoric (Z)-stilbene scaffold. All compounds were prepared on a microscale using mild, chemoselective transformations and were fully characterized by FTIR, $^{1}H/^{13}C$ NMR, and ESI-MS, confirming retention of the biologically essential *cis*-geometry.

In vitro antiproliferative evaluation using MTT and SRB assays against a panel of five human cancer cell lines (MCF-7, HeLa, A549, HCT-116, and MDA-MB-231) and the normal breast epithelial cell line MCF-10A revealed clear structure–activity relationships. Compounds CIII, CIV, CVII, and CX emerged as the most potent leads, exhibiting IC_{50} values in the range of 1.4–7.9 μM after 72 h treatment. Among them, CIII displayed the highest overall potency (IC_{50} 1.4–3.3 μM), outperforming doxorubicin in several lines, particularly breast and colorectal carcinomas. These lead compounds also demonstrated significantly improved selectivity indices (SI 7.0–22.3) compared to the reference drug doxorubicin (SI 3.8–6.3), indicating preferential toxicity toward cancer cells.

Mechanistic investigations on the top leads CIII and CVII confirmed that their anticancer activity is primarily mediated through microtubule destabilization. Both compounds potently inhibited tubulin polymerization (IC_{50} 2.6 μM for CIII and 3.9 μM for CVII), closely approaching the activity of parent CA-4. This inhibition led to pronounced dose-dependent G2/M phase arrest followed by increased sub-G1 population, characteristic of apoptotic DNA fragmentation. Flow cytometric analysis using Annexin V-FITC/PI staining further demonstrated strong induction of apoptosis via the intrinsic mitochondrial pathway, evidenced by dissipation of mitochondrial membrane potential (ΔΨm), activation of caspase-9 and executioner caspases-3/7, and nuclear morphological changes. Additionally, both leads exhibited concentration-dependent inhibition of DNA topoisomerase IIα in a decatenation assay, revealing a beneficial dual-target mechanism that may help circumvent common resistance pathways.

Conclusion

In conclusion, the rational derivatization of the B-ring of CA-4 has yielded four promising lead compounds (CIII, CIV, CVII, and CX) that effectively address several key limitations of the parent molecule, including improved potency, enhanced cancer-cell selectivity, and balanced drug-like properties while retaining strong microtubule-destabilizing activity. The identification of dual microtubule polymerization inhibition and topoisomerase IIα suppression represents an added advantage that may offer superior therapeutic potential in resistant tumor models.

This integrated approach—combining rational design, efficient microscale synthesis, comprehensive in vitro biological profiling, and multi-parametric mechanistic studies—provides a robust foundation for the further preclinical optimization and development of the CI–CX series as next-generation microtubule-targeted anticancer agents. Future studies should focus on in vivo pharmacokinetic and efficacy evaluations in xenograft models, scale-up synthesis, and exploration of combination therapies with immune checkpoint inhibitors or PARP inhibitors to fully realize the clinical potential of these promising CA-4 analogues.

References

Bukhari, S. N. A., et al. (2017). Development of combretastatins as potent tubulin polymerization inhibitors. *Bioorganic Chemistry*, 72, 130–147. https://doi.org/10.1016/j.bioorg.2017.04.007

Chen, Z. H., et al. (2023). Development of Combretastatin A-4 analogues as potential anticancer agents with improved aqueous solubility. *Molecules*, 28(4), 1717. https://doi.org/10.3390/molecules28041717

Duan, Y. T., et al. (2016). Design, synthesis and antitumor activity of novel link-bridge and B-ring modified combretastatin A-4 (CA-4) analogues as potent antitubulin agents. *Scientific Reports*, 6, 25387. https://doi.org/10.1038/srep25387

Egharevba, G. O., et al. (2022). Synthesis and characterization of novel combretastatin analogues as potential anticancer agents. *Scientific Reports*, 12, 5958. https://doi.org/10.1038/s41598-022-05958-6

Greene, L. M., et al. (2015). Combretastatins: More than just vascular targeting agents? *Journal of Pharmacology and Experimental Therapeutics*, 355(2), 212–227.

Ibrahim, T. S., et al. (2021). Discovery of novel quinoline-based analogues of combretastatin A-4 as tubulin polymerisation inhibitors with apoptosis inducing activity and potent anticancer effect. *Journal of Enzyme Inhibition and Medicinal Chemistry*, 36(1), 802–818. https://doi.org/10.1080/14756366.2021.1899168

Lin, C. M., et al. (1989). Antimitotic natural products combretastatin A-4 and combretastatin A-2: Studies on the mechanism of their inhibition of the binding of colchicine to tubulin.

Biochemistry, 28(17), 6984–6991. https://doi.org/10.1021/bi00443a031

Lv, X., et al. (2024). Dual inhibition of topoisomerase II and microtubule of podophyllotoxin derivative 5p overcomes cancer multidrug resistance. *European Journal of Pharmacology*, 980, 176857. https://doi.org/10.1016/j.ejphar.2024.176857

Malebari, A. M., et al. (2020). β-Lactams with antiproliferative and antiapoptotic activity in breast cancer cells. *European Journal of Medicinal Chemistry*, 189, 112061.

Omar, M. H., et al. (2024). Combretastatin A-4 based compounds as potential anticancer agents: A review. *Bioorganic Chemistry*, 153, 107930. https://doi.org/10.1016/j.bioorg.2024.107930

Provot, O. (2026). Who's who in the field of combretastatin A4 analogues? *European Journal of Medicinal Chemistry*. (Advance online publication).

Romagnoli, R., et al. (2012). Synthesis and evaluation of 1,5-disubstituted tetrazoles as rigid analogues of combretastatin A-4 with potent antiproliferative and antitumor activity. *Journal of Medicinal Chemistry*, 55(1), 475–488.

Singh, S. B., et al. (2024). Discovery, synthesis, activities, structure-activity relationships, and clinical development of combretastatins and analogs as anticancer drugs. *Natural Product Reports*. https://doi.org/10.1039/D3NP00053B

Yi, J. M., et al. (2015). Dual targeting of microtubule and topoisomerase II by α-carboline derivative YCH337 for tumor proliferation and growth inhibition. *Oncotarget*, 6(26), 22192–22205.

Young, S. L., et al. (2004). Combretastatin A4 phosphate: Background and current clinical status. Expert Opinion on Investigational Drugs, 13(9), 1171–1182.